Available online at www.sciencedirect.com
ScienceDirect
Journal of Molecular Graphics and Modelling 25 (2006) 363–372
Journal of Molecular Graphics and Modelling
www.elsevier.com/locate/JMGM

Binding mode analysis of the NADH cofactor in nitric oxide reductase: A theoretical study

Dóra K. Menyhárd *, György M. Keserű

Department of Chemical Information Technology, Budapest University of Technology and Economics, Gellért Tér 4., H-1111 Budapest, Hungary

Received 18 November 2004; received in revised form 10 October 2005; accepted 13 February 2006
Available online 20 March 2006

Abstract

Nitric oxide reductase (Nor), a member of the cytochrome P450 superfamily, takes part in the denitrification process of fungi by reducing NO to N_2O. Evidence indicates that Nor binds NADH, source of the reducing equivalents of the reaction, within its large hydrophilic ligand binding cavity on the distal side of heme and receives electrons directly from the cofactor. Here we present a binding mode analysis of the structure of the Nor–NO–NADH complex, performed in three steps. The NADH cofactor was first docked into the enzyme interior using the Monte Carlo multiple minimum algorithm, refined by low-mode conformational search and the final arrangement was obtained in a 5 ns NPT molecular dynamics simulation. The NADH cofactor, in our results, is positioned – by Arg174, Lys291, Asp393 and several water molecules – within reactive distance of the NO binding spot suggesting a direct hydride shift mechanism between the two. The catalytically required water molecule is captured by NADH and the cofactor not only retains the suggested H-bonded proton transfer pathway between the active site and the solvent, but provides structural restraint for its members. We also found that direct interaction is formed between the cofactor and propionate A of the heme group, which flips from the proximal to the distal side of the heme plane in order to become an H-bonding partner of NADH. The role of Arg64 and Glu71 was suggested to be fixing the residues of the translocated helix B′ to their new position.

Keywords: Heme protein; Nitrix oxide; Nitric oxide reductase; NADH; Molecular dynamics; Monte Carlo multiple minimum search; Low-mode conformational search

1. Introduction

Nitric oxide reductase (Nor) takes part in the denitrification process of certain fungi—it catalyzes the reduction of NO to N_2O [1]. The enzyme has become interesting from several points of view. Nor, although a member of the cytochrome P450 superfamily (P450s) [2], retains important structural differences which result in its inability to carry out a monooxygenation reaction characteristic of the P450s. Instead, it has a unique function of reducing NO, utilizing the same thiolate bound heme center as P450s do. The region corresponding to the substrate access channel of cytochrome P450s is in a different conformation in Nor, forming a spacious distal pocket above the heme [3] lined by an unusually large number of positively charged amino acids and filled with numerous water molecules [4]. Evidence indicates that Nor binds NADH (in case of Nor isozyme of *Fusarium oxysporum* and isozyme 1 of *C. tonkinense*, while isozyme 2 of *C. tonkinense* and isozyme of *T. cutaeum* can utilize either NADH or NADPH [5]), source of the reducing equivalents of the reaction, within this large hydrophilic ligand binding cavity thus receiving the electrons required for catalysis directly—without the aid of a reducing partner such as cytochrome P450 reductase [1]. This mode of NAD(P)H binding – e.g. capturing the cofactor in an ample cavity surrounded by a cluster of positively charged residues – is also unusual, NAD(P)H binding enzymes such as dehydrogenases typically sequester the cofactor within a Rossman fold motif [6].

The heme group of the resting state enzyme (Fe(III)Nor) binds NO in a slightly bent and tilted conformation [7]. In the presence of NAD(P)H, the complex is reduced to an intermediate (*I*) which reacts with a second NO molecule to form the N_2O product [8]:

$$\mathrm{Fe(III)Nor} + \mathrm{NO} \rightarrow \mathrm{(Fe(III)Nor)NO}$$

$$\mathrm{(Fe(III)Nor)NO} + \mathrm{NAD(P)H} \rightarrow I + \mathrm{NAD(P)^+}$$

$$I + \mathrm{NO} + \mathrm{H^+} \rightarrow \mathrm{Fe(III)Nor} + \mathrm{N_2O} + \mathrm{H_2O}$$

* Corresponding author. Tel.: +36 463 4141; fax: +36 463 3953.
E-mail address: dmenyhard@mail.bme.hu (D.K. Menyhárd).

1093-3263/$ – see front matter © 2006 Elsevier Inc. All rights reserved.
doi:10.1016/j.jmgm.2006.02.003

However, it has not been clarified yet whether the NAD(P)H mediated reduction and proton transfer occur simultaneously or sequentially, or if hydride transfer is part of the mechanism. The structure of the reaction intermediate *I* is also still under debate. Averill proposed that following hydride transfer Fe(II)NHO would be formed [9]; the results of Daibner and coworkers also support the hydride transfer mechanism and suggest an intermediate of Fe(III)·NHOH [10]. On the other hand, based on resonance Raman measurements, the Fe(II)$(NO)^{-}H^{+}$ form was suggested by Obayashi et al. [11] who argue against a hydride shift. Theoretical studies reached similar conclusions; both Tsukamoto et al. [12] and Harris [13] concluded in favor of the two electron reduced form of the initial Fe(III)NO complex (see Fig. 1). The proton required for the reaction is thought to be delivered through a hydrogen-bonding network which connects the active site and the bulk solvent, the ultimate source being an ordered water molecule bound in the immediate vicinity of NO [3,7]. Unraveling the details of the mechanism is greatly hampered by the fact that although much is known about the binding of the NAD(P)H cofactor, its exact binding mode is unclear.

Here we present a model for the ternary complex of Nor, NO and NADH. Results demonstrate that the inner landscape of Nor is architectured to hold the cofactor adjacent to the substrate leaving enough room for specific coordination of water molecules and that the heme prosthetic group also participates in the communication between the protein matrix and NADH. Our results provide a framework for further theoretical studies of the enzyme mechanism, where the effect of the cofactor could also be taken into consideration.

2. Methods

The structure of the Nor–NO–NADH complex was calculated in three steps. The NADH cofactor was first docked into the enzyme interior using the Monte Carlo multiple minimum algorithm and was further refined by low-mode conformational search. Solvent effects were modeled by using the GB/SA continuum solvation model. The structure thus derived was solvated by explicit water molecules, and the final arrangement was obtained in a 5 ns NPT molecular dynamics simulation.

2.1. Calculation of the charge set of the heme, NO and the NADH cofactor

ESP charges [14] were calculated by the B3LYP density functional method (LACVP** basis set [15]) – as implemented in the program Jaguar [16] – for the crystallographically determined geometry of the Nor(Fe(III))–NO complex (Nor of *F. oxysporum*, PDB code:1cl6 [7]). Two models were formed differing in the representation of the proximal Cys352 ligand, the residue anchoring the heme group to the protein matrix. In Model 1, an SH^{-} group, in Model 2, $CH_3CH_2S^{-}$ group was used. Both systems included five water molecules, three of these coordinate the heme propionates and two waters were found in the vicinity of the NO ligand. The carbonyl oxygen of Ala239 is 2.92 Å from the oxygen of NO, therefore an additional water molecule was built into the model to represent its effect; as in the case of the OG atom of Ser286. Since the active site of Nor is exposed to the solvent and is lined by a number of charged residues, calculations were carried out in water (using the SCRF method of Jaguar [17,18]). Charges of the NADH cofactor were obtained using the same method.

In all further calculations (carried out using the program MacroModel [19]) the heme, NO and NADH carried the charges calculated by the described protocol.

2.2. Monte Carlo multiple minimum (MCMM) search

The input structure of the MCMM search [20,21] was that of the crystal structure of the Nor–NO complex [7] with the NADH cofactor positioned manually, the internal torsions of residues 60–90, 170–180, 230–250, 282–294 (the residues building up the ligand binding pocket of Nor) and all internal torsions of NADH were considered. Monte Carlo search involved the random variation (within the range of 0°–180°) of a randomly selected subset of all torsional angles (a minimum

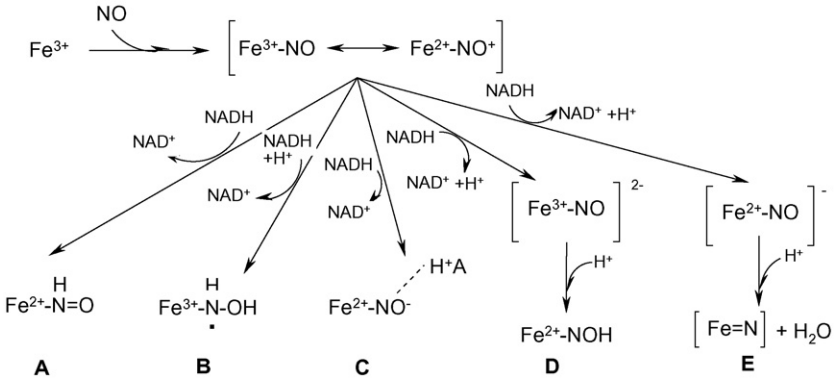

Fig. 1. Schematic representation of proposed reaction paths (A–E) leading to the formation of the reactive species (*I*) ready to attack the second NO molecule according to Averill [9], Daibner et al. [10], Obayashi et al. [11], Tsukamoto et al. [12] and by Harris [13], respectively. Schemes A and B proceed by a direct hydride shift mechanism, while in the others, donation of the hydrogen of the NADH cofactor (to a protein residue or water) will initiate a cascade leading to protonation of the active site.

of two and a maximum of 133 torsions were altered), combined with the variable molecules selection (MOLS) method for translations and rotations of the cofactor with respect to the protein bulk. The combined MCMM/MOLS procedure allowed random translation (0–3 Å) and rotation (0°–180°) of NADH with respect to the protein during a Monte Carlo step. The perturbed structures were minimized using the TNCG algorithm. The resulting minimum energy complex structures were sorted by energy, and the unique structures within a 50 kJ/mol energy window above the global minimum were stored.

Calculations were carried out using the AMBER* force field [22] and a distance dependent dielectric function with ε of 10. A flat bottom harmonic distance constraint was defined between C4 of the nicotinamide ring of NADH (C_N4) and the oxygen of NO ($r_0 = 3.3 \pm 0.4$ Å, $k = 100$ kJ/Å^2). The described setup results a restrained search where the protein matrix – aside from the listed 76 residues – was not allowed to move, and all conformers had to be such, that the C_N4 atom of NADH and the oxygen of NO are no further than 3.7 Å.

2.3. Low-mode conformational search (LMCS)

LMCS [23] was initialized from the global minimum structure of the MCMM search, using the same set of torsions. Solvent effects were modeled by the GB/SA algorithm [24]. In this search, however, the distance of the cofactor and the NO molecule was no longer constrained.

2.4. MD simulations

The global minimum structure of LMCS was subjected to a 5 ns MD simulation, removing all restrains from the system. All titratable groups were protonated according to our pK_a calculation performed on the crystal structure of the Nor–NO complex. Ionization state of the residues was calculated by ZAP, a finite-difference Poisson–Boltzmann solver available from OpenEye Scientific Software Inc. [25]. ZAP solves the Poisson–Boltzmann equation numerically using a grid-based representation in which the potential at each grid point is calculated. In contrast to other methods, however, ZAP uses a dielectric function based on atom-centered Gaussians [26] that gives a more physically realistic description of the solvent interface and results in greater stability, precision, and speed than conventional methods. Unmodified X-ray structures were shown to be best suited for the calculation when studying enzymes having no crystal contacts near their active site [27].

The simulation system for the ternary complex was set up using a cubic box of side 90 Å that includes the protein solvated with 18.237 SPC [28] water molecules. The overall charge of the protein was $-9e$; consequently, nine Na^+ ions were added to the salt solution to ensure electroneutrality of the system. The total number of atoms was 58837. All MD simulations were carried out using the GROMACS simulation suite [29] and GROMOS96 force field [30]. Application of the LINCS [31] and SETTLE [32] methods allowed for an integration step size of 2 fs. Periodic boundary conditions were applied in all simulations to avoid edge effects. The simulation was conducted at constant temperature ($T = 300$ K), pressure ($P = 1$ bar) and number of particles [33]. Solvent (i.e. water and ions) and protein were temperature-coupled separately, with a coupling constant of $\tau T = 0.1$ ps. Isotropic pressure coupling was used, with a coupling constant of $\tau P = 1.0$ ps. Numerical integration of the equations of motion used the leap-frog algorithm with a time step of 2 fs, with atomic coordinates saved every picosecond for analysis. Energy minimizations were performed using a steepest descent algorithm.

Aliphatic groups in the protein were treated with the united atom representation. The van der Waals interactions were modelled using a 6–12 Lennard–Jones (LJ) potential, cut off at 10 Å, with first- and second-neighbour exclusions and scaled third-neighbour LJ coefficients. Electrostatic interactions were computed using the Particle–Mesh Ewald algorithm [34], with a 9 Å cut-off for the direct space calculation; the reciprocal space calculation was performed using a fast Fourier transform (FFT) algorithm. The simulation was performed on a HP Proliant DL560 Linux server, using four parallel 2.5 GHz Pentium4 Xeon processors; the CPU time was approximately 50 h/ns.

The simulation started from the global minimum (GM) structure of the LMCS calculation with an energy minimization using a steepest descent algorithm (nstep = 1000; emtol = 1000.0; emstep = 0.01 steps) and was followed by simulation of 200 ps length with harmonic position restraints applied on all protein atoms (force constant 1000 kJ/mol/Å^2) to allow relaxation of the solvent molecules. Five nanosecond NPT molecular dynamics simulation was started from the energy minimized structure of Nor–NO–NADH complex produced by the corresponding position restrained simulation. The coordinates of the system were stored after every 500 steps to yield a total of 5000 sampled conformations for the trajectory, having excluded the first 500 ps which was regarded as the equilibration period.

3. Results

3.1. DFT charge calculations

Calculated charge set for the heme cofactor and the NO molecule of the Nor(Fe(III))–NO state, and of the NADH cofactor are summarized in Table 1 and Fig. 2. The use of two different representations of the proximal residue anchoring the heme group to the protein matrix was necessary since

Table 1
Atomic charge (ρ) and spin densities (σ) of the solvated heme–NO complex summed into fragments

	Model 1		Model 2	
	ρ	σ	ρ	σ
Fe	0.362	−1.179	0.519	−1.238
Protoporhyrin IX	−1.825	0.084	−1.859	0.099
N of NO	0.077	0.643	−0.009	0.663
O of NO	−0.032	0.344	−0.016	0.356
S^- of proximal Cys	−0.594	0.112	−0.548	0.117

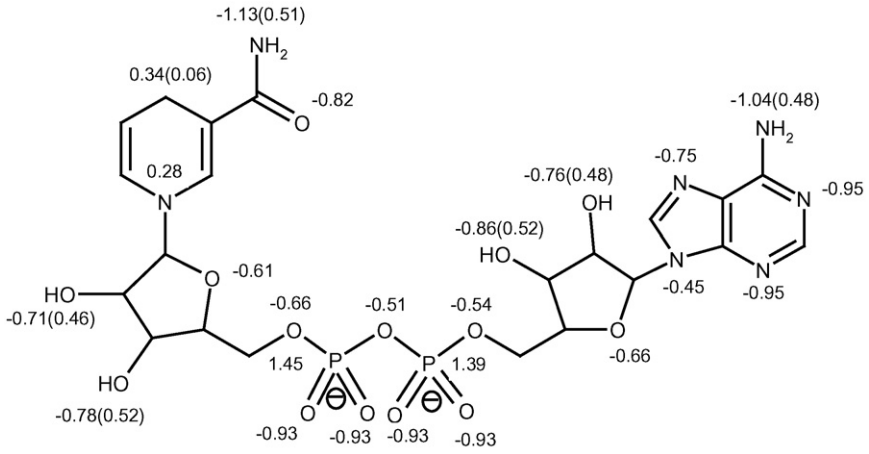

Fig. 2. Characteristic atomic charges of the water solvated NADH cofactor (hydrogen charges are shown in parentheses for functional groups).

theoretical results were shown to depend on this feature; SH^- was shown to give a better approximation of electron affinities, bond energies and spin densities of, especially, the high oxidation states of P450s than the other frequently chosen Cys^- model, CH_3S^- in calculation systems lacking the proximal H-bond network coordinating the cysteinato S^- [35]. In Nor also, quite similarly to that seen in P450s, three NH. . .S type H-bonds (Ile353, Ala354 and Glu355 interacting with S^- of Cys352) and an NH. . .O type (formed between NH of Cys252 and the carbonyl group of Phe345) contribute to the stabilization of the negative charge of S^-. Results using the SH^- model were compared with those derived using the electron donating methyl substituent, and we found that charges of the NO ligand are small in both cases, and – based on the spin density motif – the same conclusion, as to the overall electronic state of the complex, can be drawn. As it can be seen, according to our calculations the geometry of the Nor–NO complex is in accordance with the "Fe^{3+}–NO" form with a near neutral NO molecule and considerable electron donation from the thiolate axial ligand, using either model system.

3.2. MCMM calculation

Since the ligand-binding cavity of Nor is extended and the cofactor can well be supposed to assume several binding modes within it [36], we reviewed the structural criteria of forming an active complex. Fourteen such structures of NADH and a substrate in a ternary complex (mostly dehydrogenases and one reductase enzyme) were found in the Protein Data Bank. In 96% of the 28 NADH–substrate interactions found, the distance of C_N4 of NADH and the corresponding electron acceptor was within the 3.3 ± 0.4 Å. Therefore, this same constraint was applied in the first set of our calculations—a crude docking of the cofactor within the enzyme interior. A 500 step MCMM search afforded 65 low energy conformers within a 50 kJ/mol energy window from the global minimum (GM) of the calculation. GM and the conformation 2 are well separated in energy from the rest (relative potential energy of the first eight conformers: 0.00, 2.44, 13.02, 15.29, 15.64, 16.01, 17.32, 18.28 kJ/mol). The two structures are very similar, with an rms distance for all moving atoms of 1.26 Å. The most significant difference between the two is in a 180° flip of the amide group of the nicotinamide part. Distance of the C_N4 atom of NADH and the oxygen of NO (constrained to the 2.9–3.7 Å interval) was 2.98 and 3.03 Å in the GM and in conformer 2, respectively. Compared with the crystal structure, docking the NADH cofactor caused greatest shift of residues 63–82 (average C_α-shift = 3.16 Å, maximum C_α-shift = 4.64 Å (at Ala80)) and 172–178 (average C_α-shift = 4.77 Å, maximum C_α-shift = 7.68 Å (at Arg174)). In the GM conformer the cofactor is coordinated by 12 intermolecular H-bonds, the nicotinamide ring is H-bonded by Thr175, the pyrophosphate region by Arg64, Arg174 and Lys291, while the adenine nucleotide by Leu72, Ser175 and Asn176.

3.3. LMCS calculations

LMCS was conducted on the GM structure of the MCMM analysis. Results are summarized in Table 2. In this run, just as in the previous, two low energy structures separate from the rest. The two low-energy structures are almost identical, with the greatest difference of a 0.49 Å shift of the NH_2 group of the nicotinamide ring which results in a switch of H-bonding partners as well (in the GM structure OG of Thr175, in conformation 2, the backbone carbonyl oxygen of Arg174 coordinates this part of the molecule). In the GM structure the cofactor is held by 14 H-bonds. The central pyrophosphate moiety is H-bonded to Arg64, Arg174 and Lys291, just as in the

Table 2
Summary of the results of LMCS

Conformation	Energy (kJ/mol)	Relative energy (kJ/mol)
1 (GM)	−33945.039	0.000
2	−33940.715	0.789
3	−33930.418	10.297
4	−33916.773	23.941
5	−33911.430	29.285
6	−33909.512	31.203
7	−33906.859	33.855
8	−33896.918	43.797

MCMM derived model; however a new contact between the heme and NADH has formed. Propionate A became H-bonded by one of the ribose OH groups. An ionic interaction has formed between the positively charged C_N4 atom of the nicotinamide ring and the backbone carbonyl of Ala239, which is H-bonded to the NH1 nitrogen of Arg174. Therefore, Arg174, indirectly, fixed the nicotinamide part of the cofactor also.

3.4. MD simulations

Solvation with explicit water molecules and removal of all constraints from the structure resulted in an arrangement similar to that derived by LMCS. The center-of-mass of the cofactor has moved by 0.59 Å, with the largest difference in the position of the NH_2 group of the adenine ring (4.95 Å), where solvent might have the greatest effect. Average distance between NO and C_N4 of NADH was found to be 3.09 Å. The group reaching closest to NO was the backbone carbonyl of Ala239, 2.98 Å from the oxygen, 3.37 Å from C_N4.

In the crystal structure residues 73–80, 126–139, 176–180, 203–209 and those after 367 were found to have greater than average thermal factors, corresponding to the increased flexibility of helix B′ and three surface close loops, those of loop D–E, loop F–G and loop G–H, and the terminal region. As it can be seen on Fig. 3A, the MD trajectory retained similar tendencies, however two characteristic differences are visible at first sight: the B′ helix and loop F–G (connecting helices F and G) became quite a bit more ordered. Both of these are situated at the entrance of the large substrate/cofactor binding cleft, and both were foreseen to interact with molecules bound within [36].

The average structure of the equilibrated trajectory is shown on Fig. 4. When compared with the crystal structure of the Nor–NO complex, the most notable deviations in C_α positions can be seen for residues 72–76, 104–109 and 173–180, as shown on Fig. 3B. Fig. 3B also shows calculated thermal factors along the backbone, and it can be seen that, especially in the 72–76 (members of helix B′) and the 173–180 regions of the sequence, deviation from the crystal structure is coupled to low thermal factor values, therefore the restructuring in these segments cannot simply be the result of solvation induced increased mobility. We consider the rearrangement of these two regions as the characteristic conformational change associated with NADH binding. Calculated thermal factors within the cofactor and the prosthetic group were well below average, aside from the adenine ring of NADH, which has a conformational freedom on the scale of an average amino acid (data not shown).

The mobility of solvent water molecules was also analyzed. Average thermal factor of water molecules was more than 35

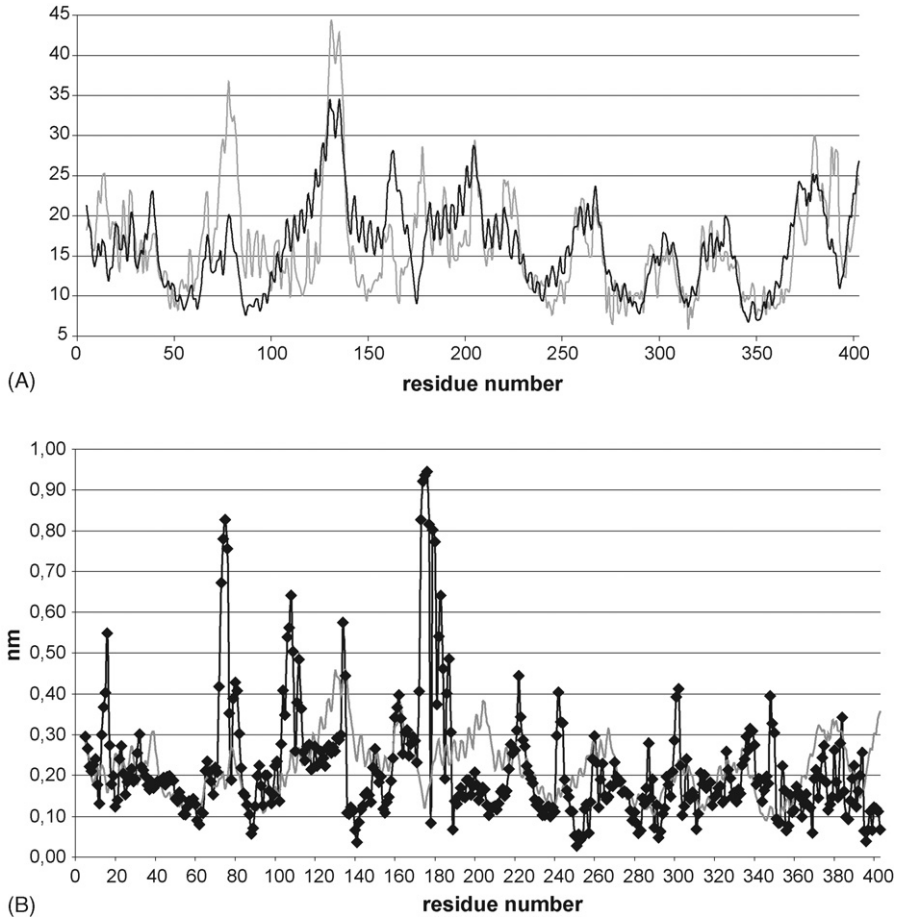

Fig. 3. Panel A: Comparison of the thermal factors of the Nor–NO complex (light grey line) with those calculated in the MD simulation-scaled to fit the graph by the ratio of the respective average values (black line). Panel B: Black squares: C_α deviation of the average structure of the equilibrated MD trajectory and the crystal structure of the Nor–NO complex (pdb code: 1cl6), grey line: calculated thermal factors (scaled to fit the graph by the ratio of the respective average values).

Fig. 4. Calculated structure of the Nor–NO–NADH ternary complex and the ordered water molecules associated to the complex (heme atoms are colored yellow, waters are represented by red spheres).

times higher than those of the protein residues, however, of the 18237 water molecules, 20 had similar thermal factors to the protein matrix. Ten ordered water molecules were found within the cofactor-binding cleft, six of them within 3.4 Å of NADH. These, together with all H-bonding contacts are shown on Fig. 5. Fig. 6 shows the H-bonding distances of some characteristic partners of NADH. In 91% of all snapshots of the equilibrated trajectory Arg174 is directly bound to the pyrophosphate moiety of NADH, in 50% of the cases this means at least two H-bonds. In 85% of the structures Lys291 is H-bonded to an oxygen of the pyrophosphate region, in 31% of the cases, to two. H-bonds are formed between Asp393 and the ribose OH groups of the adenine nucleotide; in 98% of the structures OD1 or OD2 is linked to a ribose OH, in 96% of the cases, to both. A low-thermal-factor water is captured above the nicotinamide ring within 4 Å of the C_N4 atom in 97% of the snapshots, fixed by an H-bond from the amide group of the ring in 91% of the cases.

In the crystal structure of Nor–NO [7], propionate D of the heme is coordinated by three water molecules, two histidines (His94, His350) and Arg98; in the average structure of the simulation contact with His350 was lost, however the propionate oxygens were found H-bonded by His94, Arg98 and also by three low-thermal-factor water molecules. Propionate A, on the other hand, flipped from the proximal side of the heme plane to the distal, ligand binding face and coordinated – in almost all structures of the equilibrium trajectory – a ribose OH at the nicotinamide part of the cofactor. In 99% of all structures an H-bond is established between one of the carboxyl oxygens of propionate A and a ribose OH, in 44% of the structures both carboxyl oxygens take part in the interaction (see Fig. 6). Conserved Arg292 stayed coordinated to propionate A via an ordered water molecule.

In the average structure of the equilibrium trajectory there is only one direct H-bonding interaction between the shifted helix B′ (residues 73–80) and NADH (an H-bond between OG of Ser75 and one of the pyrophosphate oxygens), however in individual snapshots an extensive interaction can be seen via several water molecules (Fig. 7 shows an example). In this region the water molecules are rapidly exchanging due the proximity of the bulk solvent. Average distance of Ser73 OG oxygen, its backbone carbonyl, or the OG oxygen of Ser75 and oxygens of the pyrophosphate moiety, however, are well below 4.5 Å throughout the trajectory.

Arg64 and Glu71 both take part in the fixing helix B′ in its new position. Agr64 H-bonds, through its NH_2 nitrogen, the backbone carbonyl of Ser75; while Glu71 coordinates the backbone amide group of several members of helix B′, those of Ser75, Gly76, Lys77 and Gln78. Direct interaction between Arg64 and Asp88 (part of a characteristic salt-bridge network) was broken, with the closest atom pair of NE1 of Arg64 and

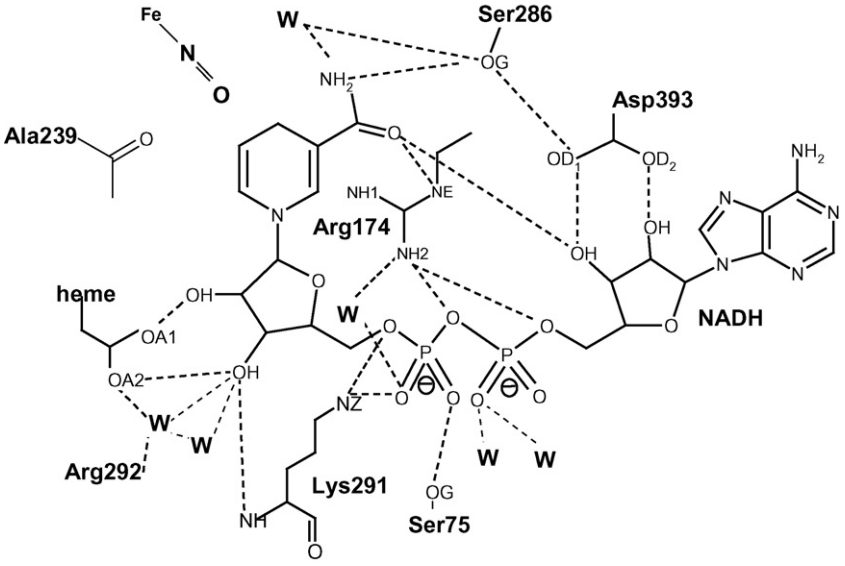

Fig. 5. H-bonding pattern around the NADH cofactor in the average structure of MD.

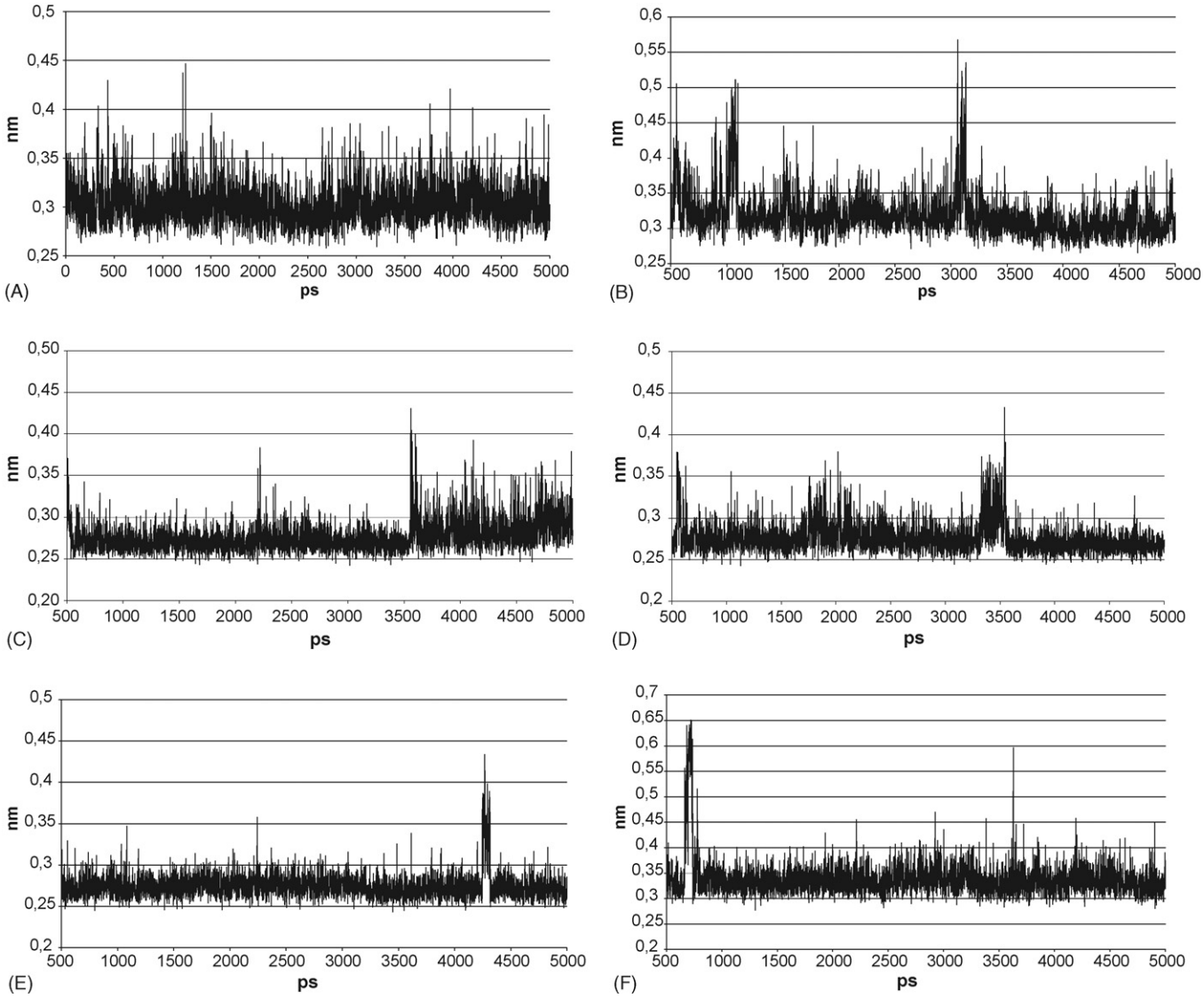

Fig. 6. H-bonding partners of NADH along the equilibrated trajectory of the MD simulation. The distance between Arg164 nitrogen and the closest reaching oxygen of the pyrophosphate moiety (Panel A), the closest oxygen of the pyrophosphate moiety and NZ of Lys291 (Panel B), the closer ribose OH of the adenine nucleotide and OD1 or OD2 of Asp393, respectively (Panel C and D), the closer reaching carboxyl oxygen of propionate A of the heme and the ribose OH of the nicotinamide part of the cofactor (Panel E) and that of the ordered water molecule and C_N4 of the nicotinamide ring (Panel F).

OD1 of Asp88, 3.9 Å apart. However, in individual snapshots, reflecting the effect of neighboring bulk solvent, rapidly exchanging water molecules provide indirect connection between the two.

4. Discussion

The overall fold of Nor, mostly made up of α-helical segments, is very similar to that of the monooxygenase P450s, except that helices F, G and B′ flip and thus create a large cavity at the distal heme side [3]. This results in a pronounced change in function also, Nor receiving electrons from the distal instead of the proximal side – as in case of P450 monooxygenases – catalyses the two electron reduction of NO at he heme site. The heme is held between the distal I and proximal L helices anchored by a Cys residue. According to our results, the NO molecule in – Nor(Fe(III))–NO-initial complex of the catalytic cycle – is near neutral, due to the fact that the strong axial ligand of thiolate enhances electron back-donation from the iron to NO and discourages electron flow from the ligand. This is reflected by experimental results also, in a unique binding mode [7] of the slight bend and tilt for NO and an N–O stretching frequency of the complex at 1851 cm^{-1}, near that of free NO [37]. The electron donating cofactor of the reaction, NADH, was shown to bind within the spacious ligand binding cavity by mutation studies, where a number of charged amino acids exert crucial influence on its binding conformation and efficiency [4]. Since NO itself does not carry a pronounced charge, protein-cofactor contacts have to orient the cofactor within the proximity of it so, by electron transfer between the two, the reaction intermediate could be formed. It was also shown that even in the absence of NO, Nor forms reversible complexes with the electron donating cofactors [36,38].

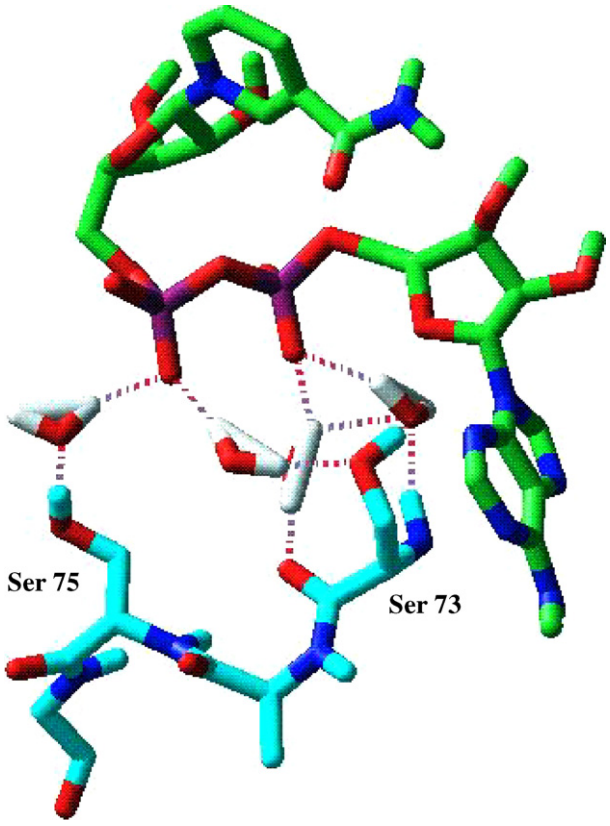

Fig. 7. Interaction between members of helix B′ and the NADH cofactor in the structure belonging to the 3 ns snapshot of the MD trajectory. (Carbons and hydrogens of NADH are colored green, carbons and hydrogens of helix B1 are colored cyan.)

Results show that NADH – coordinated by numerous H-bonds – is held tight within the large, distal side cavity of Nor, positioned 3 Å away from the NO molecule. Their proximity and the fact that no other plausible electron transfer components are present within the active site definitely suggests that electron donation from the cofactor proceeds by a direct hydride shift mechanism. This is in accord with the first proposal for the reaction mechanism [9], and is also supported by experimental results such that intermediate formation could be evoked by borohydride addition and by pulse radiolysis generated $^{\bullet}$NHOH radical [10], or by the recently published structure of the binary complex of a NADH analogue and Nor where the cofactor was captured right above the heme plane [39]. The proposed hydride shift mechanism was challenged, on one hand by Raman spectroscopic results which failed to detect an exchangeable proton on the N of NO in the reaction intermediate (although did not exclude the possibility of weak H-bonding on NO) [11] and also by theoretical studies that suggested the two electron reduced ferric NO complex as the reaction intermediate [12,13]—however, the model systems considered did not include any representation of the cofactor. Since hydride transfer across a water molecule is unlikely to occur [11], NO itself is the only suitable hydride ion acceptor according to our results.

Binding of the cofactor results in rearrangement of helix B′ (residues 73–80), shown to participate in cofactor differentiation [36], and in the region connecting helices G and H (residues 173–178). These two regions form the entrance of the large cavity of Nor, and ligation of NADH initiates their movement toward the cofactor inducing both a new position and restrained mobility to these segments. In our ternary model, the binding mode of NADH is curved, an intra-molecular H-bond between the amide group of the nicotinamide ring and the ribose OH of the adenine nucleotide pulls the two ends of the molecule toward each-other. Nevertheless, the adenine nucleotide segment reaches into the solvent, while the nicotinamide ring is buried adjacent to the heme group. Within the curve – in a central position – Arg174 anchors the molecule to the protein matrix, NE of Arg174 coordinates the oxygen of the amide group while its NH1 or NH2 nitrogens form, in the majority of cases, three H-bonds with the pyrophosphate moiety, two direct interactions and one via an ordered water molecule. From the opposite side, Lys291 interacts with the cofactor; the NZ nitrogen forms two contacts with the pyrophosphate region and a further H-bond toward the ribose OH of the nicotinamide part.

Mutations of the positively charged residues of the inner distal pocket, those of Lys62, Arg64, Arg174, Lys291, Arg292, were all shown to modulate Nor activity, of these, in accordance with our results, Arg174 was shown to be crucial in cofactor coordination [4]. R174E and R174Q mutants were both shown to disengage formation of the intermediate (*I*) of the reduction step due to loosing NADH binding ability. Mutations at positions 62, 64, 291 and 292 resulted in different extent of decrease in overall activity caused by slowing intermediate formation. Of these Arg64 was considered most significant since it is located just opposite from Arg174 on the facing side of the ligand binding cleft, positioned ideally to collaborate with Arg174 in fixing a negatively charged moiety [4]. Although when using a restrained model (MCMM, LMCS calculations) we found Arg64 coordinated to the pyrophosphate region of the cofactor, in the MD simulation, its side-chain flipped out toward the solvent. Its place, in our results, was taken by its close – through space – neighbor, Lys291. Arg64, together with Glu71 took part in the stabilization of helix B′ in its new position and thereby influence closing of the entrance region of the ligand binding cavity upon cofactor ligation. Arg64 and Glu71 are part of a salt-bridged triad (Glu71–Arg64–Asp88) in the resting state and NO bound Nor structures [3,7] which broke up in our ternary model. Significance of Glu71, according to our results, might be attributed to fixing the members of helix B′ and thus hindering the exit of the cofactor—reforming of the triad would result in liberation of helix B′ and acceleration of cofactor release. Observations such that E71A mutation impairs enzyme function by blocking NADH binding [40], or that in D88A and D88V mutants Nor activity considerably decreased through impairing NAD^+ release [38] further support our results.

Both ribose moieties of NADH are coordinated by several H-bonds, beside those already mentioned, the ribose OH groups of the adenine part are held by two strong H-bonds from Asp393 which was shown in a mutation study to play important role in interaction with NADH [38]. On the other hand, the ribose OH groups of the nicotinamide part H-bond one of the

heme propionates which is quite significant since even slight modifications in propionate conformation were shown to influence heme redox potential – although not by a great extent [41] – however in this case a characteristic conformational change takes place which results in an over 3 Å shift of the carboxylate moiety, and rearrangement of its H bonding interactions.

Beside the binding conformation of the cofactor, another intriguing question is the source of the proton required for catalysis. The most probable source of this proton was shown to be an ordered water molecule preferably bound in the vicinity of NO [7,38]. Such a water molecule was located in the Nor–NO complex, and was found to be connected to the solvent by the water–Ser286–water–Asp393 H-bonded network. Lack of water at this position was shown to be the direct cause of enzyme inhibition in Ser286 mutants [7]. We found 10 ordered water molecules within the ligand-binding cavity of the MD derived ternary complex. A water molecule, with very low thermal factor, was found associated to the positive charge of the C_N4 of NADH and H-bonded by its amide group. This water molecule did not form an H-bond with NO (since the NO oxygen did not carry a negative charge), however once the substrate is reduced, it has to shift <1 Å to be an ideally positioned proton donor. This water molecule was also bound by Ser286, which, in our model, forms a direct H-bond with Asp393. Therefore the proposed Ser286/Asp393 proton transfer pathway is retained and reinforced in the presence of the cofactor also.

The crystal structure of a double mutant form of Nor (S73G, S75G) in complex with 3-pyridine aldehyde adenine dinucleotide (PAAD), which – in 80% of the cases – oxidized to nicotinic acid pyridine dinucleotide (NAAD), has been published recently [39]. (The deposited crystal structure was withdrawn and re-deposited with a new pdb code of 1xqd.) Although grave differences exist between the studied systems – that of the absence of the NO ligand in the crystal structure, the different functional groups of the nicotine ring and the apolar substitutions in the B′ helix of Nor – several similarities of the crystal structure and our computational model can be found. The cofactor, in both cases, was bound in the heme-distal pocket, within the ample ligand binding cavity with the nicotinamide (or nicotinic acid) ring reaching over the heme plane and the adenine nucloeotide to the solvent. Binding of NAAD caused greatest rearrangement of the B′ helix and the backbone structure around Arg174, just as seen in our final model. Arg174 was confirmed by both studies as key interacting residue of the protein matrix of the complex. The Asp88. . .Arg64 H-bond was disrupted, while H-bond connection between the conserved Arg292 and the heme propionate was maintained in both studies. In the crystal structure the upward shift of propionate A was detected, but direct interaction between the cofactor and the heme group – such in our calculation – was not. Results also disagree as to the role of Arg64, which according to the crystallographic result takes part in direct coordination of the cofactor. In the NAAD complex of the double mutant Nor, most likely due to the altered functional group of the nicotinamide ring, the proton transfer pathway between the active site and the solvent was destabilized by insertion of a further water molecule between Ser286 and Asp393. Water molecules were expelled from the proximity of the ligand binding spot of NO, and it is the OH group of Ser286 that reaches closest to the C_N4 atom of NAAD (and the expected position of the NO ligand), however Ser286 is unlikely to be the ultimate source of the catalytically required proton [7]. Since our theoretical approach permitted us the use of physiological cofactor, wild type sequence and allowed for the presence of NO – crucial participant of the catalytic complex – we feel, though agreeing on the basic mode of binding, our results might clarify the details of the cofactor-protein interactions.

5. Conclusion

Nor, unlike the other members of the P450 family, captures its electron donating partner, NADH, within its heme containing spacious ligand binding cavity. The entrance region, especially residues of helix B′, close on the bound cofactor. NADH is positioned – by Arg174, Lys291, Asp393 and several water molecules – within reactive distance of the NO binding spot. Besides electron donation, the cofactor fulfills unique functions. NADH secures the water molecule that might be the ultimate source of the proton required for catalysis and not only retains the H-bonded proton transfer pathway between the active site and the solvent, but provides structural restraint for its members. The cofactor also forms direct interaction the with heme group via propionate A and thereby might exert influence over heme reactivity. These observations should contribute to the debate on the reaction mechanism by providing a renewed framework for theoretical considerations.

Acknowledgement

This work was supported by the Hungarian Scientific Research Fund (OTKA Grant No. T042933). DKM is a Zoltán Magyary Postdoctoral fellow.

References

[1] K. Nakahara, T. Tanimoto, K. Hatano, K. Usuda, H. Shoun, Cytochrome P450 55A1 (P450dNIR) acts as nitric oxide reductase employing NADH as the direct electron donor, J. Biol. Chem. 268 (1993) 8350–8355.
[2] H. Kizawa, D. Tomura, M. Oda, A. Fukamizu, T. Hoshino, O. Gotoh, T. Yasui, H. Shoun, Nucleotide sequence of the unique nitrate/nitrite-inducible cytochrome P450 cDNA from *Fusarium oxysporum*, J. Biol. Chem. 266 (1991) 10632–10637.
[3] S.Y. Park, H. Shimizu, S. Adachi, A. Nakagawa, I. Tanaka, K. Nakahara, H. Shoun, E. Obayashi, H. Nakamura, T. Iizuka, Y. Shiro, Crystal structure of nitric oxide reductase from denitrifying fungus *Fusarium oxysporum*, Nat. Struct. Biol. 4 (1997) 827–832.
[4] T. Kudo, N. Takaya, S.Y. Park, Y. Shiro, H. Shoun, A positively charged cluster formed in the heme-distal pocket of cytochrome P450Nor is essential for interaction with NADH, J. Biol. Chem. 276 (2001) 5020–5026.
[5] L. Zhang, N. Takaya, T. Kitazume, T. Kondo, H. Shoun, Purification and cDNA cloning of nitric oxide reductase cytochrome P450Nor (CYP55A4) from Trichosporon cutaneum, Eur. J. Biochem. 268 (2001) 3198–3204.

[6] M.G. Rossmann, D. Moras, K.W. Olsen, Chemical and biological evolution of nucleotide-binding protein, Nature 250 (1974) 194–199.
[7] H. Shimizu, E. Obayashi, Y. Gomi, H. Arakawa, S.Y. Park, H. Nakamura, S. Adachi, H. Shoun, Y. Shiro, Proton delivery in NO reduction by fungal nitric-oxide reductase. Cryogenic crystallography, spectroscopy, and kinetics of ferric–NO complexes of wild-type and mutant enzymes, J. Biol. Chem. 275 (2000) 4816–4826.
[8] Y. Shiro, M. Fujii, T. Iizuka, S. Adachi, K. Tsukamoto, K. Nakahara, H. Shoun, Spectroscopic and kinetic studies on reaction of cytochrome P450Nor with nitric oxide. Implication for its nitric oxide reduction mechanism, J. Biol. Chem. 270 (1995) 1617–1623.
[9] B.A. Averill, Dissimilatory nitrite and nitric oxide reductases, Chem. Rev. 96 (1996) 2951–2964.
[10] A. Daiber, T. Nauser, N. Takaya, T. Kudo, P. Weber, C. Hultschig, H. Shoun, V. Ullrich, Isotope effects and intermediates in the reduction of NO by P450(Nor), J. Inorg. Biochem. 88 (2002) 343–352.
[11] E. Obayashi, S. Takahashi, Y. Shiro, Electronic structure of reaction intermediate of cytochrome P450Nor in its nitric oxide reduction, J. Am. Chem. Soc. 120 (1998) 12964–12965.
[12] K. Tsukamoto, S. Nakamura, K. Shimizu, SAM1 semiemperical calculations on the catalytic cycle of nitric oxide reductase from *Fusarium oxysporum*, J. Mol. Struct. (THEOCHEM) 624 (2003) 309–322.
[13] D.L. Harris, Cytochrome P450Nor: a nitric oxide reductase-structure. Spectra and mechanism, Int. J. Quant. Chem. 288 (2002) 183–200.
[14] R.J. Woods, M. Khalil, W. Pell, S.H. Moffat, V.H. Smith Jr., Derivation of net atomic charges from molecular electrostatic potentials, J. Comput. Chem. 11 (1990) 297–310.
[15] P.J. Hay, W.R. Wadt, Ab initio effective core potentials for molecular calculations. Potentials for the transition metal atoms Sc to Hg, J. Chem. Phys. 82 (1985) 299–310.
[16] Jaguar, Version 4.1, Schrödinger Inc., Portland, OR.
[17] D.J. Tannor, B. Marten, R. Murphy, R.A. Friesner, D. Sitkoff, A. Nicholls, M. Ringnalda, W.A. Goddard III, B. Honig, Accurate first principles calculation of molecular charge distributions and solvation energies from Ab initio quantum mechanics and continuum dielectric theory, J. Am. Chem. Soc. 116 (1994) 11875–11882.
[18] B. Marten, K. Kim, C. Cortis, R.A. Friesner, R.B. Murphy, M.N. Ringnalda, D. Sitkoff, B. Honig, New model for calculation of solvation free energies: correction of self-consistent reaction field continuum dielectric theory for short-range hydrogen-bonding effects, J. Phys. Chem. 100 (1996) 11775–11788.
[19] F. Mohamadi, N.G.J. Richards, W.C. Guida, R. Liskamp, M. Lipton, C. Caufield, G. Chang, T. Hendrikson, W.C. Still, MacroModel-an integrated software system for modeling organic and bioorganic molecules using molecular mechanics, J. Comput. Chem. 11 (1990) 440–467.
[20] G. Chang, W.C. Guida, W.C. Still, An internal-coordinate Monte Carlo method for searching conformational space, J. Am. Chem. Soc. 111 (1989) 4379–4386.
[21] M. Saunders, K.N. Houk, Y.D. Wu, W.C. Still, M. Lipton, G. Chang, W.C. Guida, Conformations of cycloheptadecane. A comparison of methods for conformational searching, J. Am. Chem. Soc. 112 (1990) 1419–1427.
[22] (a) S.J. Weiner, P.A. Kollman, D.A. Case, U.C. Singh, C. Ghio, G. Alagona, S. Profeta, P. Weiner, A new force field for molecular mechanical simulation of nucleic acids and proteins, J. Am. Chem. Soc. 106 (1984) 765–784;
(b) G.M. Keserű, I. Kolossvary, B. Bertók, Cytochrome P450 catalyzed insecticide metabolism. Prediction of regio and stereoselectivity in the primer metabolism of carbofuran: a theoretical study, J. Am. Chem. Soc. 119 (1997) 5126–5131.
[23] I. Kolossváry, W.C. Guida, Low-mode search. An efficient, automated computational method for conformational analysis: application to cyclic and acyclic alkanes and cyclic peptides, J. Am. Chem. Soc. 118 (1996) 5011–5019.
[24] W.C. Still, A. Tempczyk, R.C. Hawley, T. Hendrickson, Semianalytical treatment of solvation for molecular mechanics and dynamics, J. Am. Chem. Soc. 112 (1990) 6127–6129.
[25] ZAP, OpenEye Scientific Software Inc., Santa Fe, NM.
[26] J.A. Grant, B.T. Pickup, A. Nicholls, A smooth permittivity function for poisson-boltzmann solvation methods, J. Comput. Chem. 22 (2001) 608–640.
[27] J.E. Nielsen, J.A. McCammon, On the evaluation and optimisation of protein X-ray structures for pK_a calculations, Protein Sci. 12 (2003) 313–326.
[28] H.J.C. Berendsen, J.P.M. Postma, W.F. von Gunsteren, J. Hermans, in: B. Pullman (Ed.), Intermolecular Forces, P331, Reidel, Dordrecht, 1981.
[29] E. Lindahl, B. Hess, D. van der Spoel, GROMACS 3.0: a package for molecular simulation and trajectory analysis, J. Mol. Model. 7 (2001) 306–317.
[30] W.F. van Gunsteren, S.R. Billeter, A.A. Eising, P.H. Hunenberger, P. Kruger, A.E. Mark, W.R.P. Scott, I.G. Tironi, Biomolecular Simulation: The GROMOS96 Manual and User Guide, vdf Hochschulverlag AG an der ETH Zurich, 1996.
[31] B. Hess, H. Bekker, H.J.C. Berendsen, J.G.E.M. Fraaije, LINCS: a linear constraint solver for molecular simulations, J. Comp. Chem. 18 (1997) 1463–1472.
[32] S. Miyamoto, P.A. Kollman, An analytical version of the SHAKE and RATTLE algorithms for rigid water models, J. Comp. Chem. 13 (1992) 952–962.
[33] H.J.C. Berendsen, J.P.M. Postma, W.F. van Gunsteren, A. DiNola, J.R. Haak, Molecular dynamics with coupling to an external bath, J. Chem. Phys. 81 (1984) 3684–3690.
[34] T. Darden, D. York, L. Pedersen, Particle mesh Ewald: an $N \log(N)$ method for Ewald sums in large systems, J. Chem. Phys. 98 (1993) 10089–10092.
[35] F. Ogliaro, S.P. de Visser, S. Cohen, P.K. Sharma, S. Shaik, Searching for the second oxidant in the catalytic cycle of cytochrome P450: A theoretical investigation of the iron(III)–hydroperoxo species and its epoxidation pathways, J. Am. Chem. Soc. 124 (2002) 2806–2817.
[36] L. Zhang, T. Kudo, N. Takaya, H. Shoun, The B′ helix determines cytochrome P450Nor specificity for the electron donors NADH and NADPH, J. Biol. Chem. 277 (2002) 33842–33847.
[37] E. Obayashi, K. Tsukamoto, S. Adachi, S. Takahashi, M. Nomura, T. Iizuka, H. Shoun, Y. Shiro, Unique binding of nitric oxide to ferric nitric oxide reductase from *Fusarium oxysporum* elucidated with infrared, resonance Raman, and X-ray absorption spectroscopies, J. Am. Chem. Soc. 119 (1997) 7807–7816.
[38] M. Umemura, F. Su, N. Takaya, Y. Shiro, H. Shoun, D88A mutant of cytochrome P450Nor provides kinetic evidence for direct complex formation with electron donor NADH, Eur. J. Biochem. 271 (2004) 2887–2894.
[39] R. Oshima, S. Fushinobu, F. Su, L. Zhang, N. Takaya, H. Shoun, Structural evidence for direct hydride transfer from NADH to cytochrome P450Nor, J. Mol. Biol. 342 (2004) 207–217.
[40] F. Su, S. Fushinobu, N. Takaya, H. Shoun, Involvement of a Glu71–Arg64 couple in the acess channel of NADH in cytochrome P450Nor, Biosci. Biotechnol. Biochem. 68 (2004) 1156–1159.
[41] Z. Chen, T.W.B. Obst, J.P.M. Schelvis, Phe393 mutant of cytochrome P450 BM3 with modified heme redox potentials have altered heme vinyl and propionate conformations, Biochemistry 43 (2004) 1798–1808.